Case Studies in Construction Materials 18 (2023) e01828

Contents lists available at ScienceDirect

Case Studies in Construction Materials

journal homepage: www.elsevier.com/locate/cscm

Case study

Acoustical properties of compressed earth blocks: Effect of compaction pressure, water hyacinth ash and lime

Justus Ouma [a], Nicholas Ongwen [a,b,*], Erick Ogam [c], Mercy Auma [a], Z.E.A. Fellah [c], Maxwell Mageto [d], Mohamed Ben Mansour [e], Andrew Oduor [a]

[a] Maseno University, P.O. Box Private Bag, Maseno, 40137, Kenya
[b] Tom Mboya University College, P.O. Box 199, Homa-Bay, 40300, Kenya
[c] Laboratoire de Mécanique et d'Acoustique, LMA-UMR 7031 Aix-Marseille University-CNRS-Centrale Marseille, F-13453 Marseille CEDEX 13, France
[d] Masinde Muliro University of Science and Technology, P.O. Box 190, Kakamega 50100, Kenya
[e] Laboratoire d'Énergétique et des Transferts Thermique et Massique, Faculté des Sciences de Bizerte, Université de Carthage, Tunisia

ARTICLE INFO

Keywords:
Compressed earth blocks
Acoustics of compressed earth blocks
Water hyacinth in compressed earth blocks
Lime-stabilized earth blocks

ABSTRACT

This study assessed the potential use of a mixture of lime and water hyacinth ash (WHA) as binders in fabrication of cylindrical compressed earth blocks (CEBs) with good acoustic absorption properties for building and construction. Different concentrations of the binders and compaction pressures were employed so as to vary the acoustical properties of the fabricated blocks. The geometric and transport parameters of their porous microstructure were recovered through probing using acoustic waves. A low-frequency acoustic wave guide was built for this purpose. It was found out that the transmission coefficient decreased with the compaction pressure, and with addition of lime, while WHA increased the transmission coefficient. The non-acoustical parameters recovered using the equivalent fluid model (JCAL) showed that the variation of the geometry of the microstructure of the blocks is what influences the acoustic transmission coefficient. Thus, the properties of the CEBs can be steered using binder concentration and compaction pressure in a controlled manner.

1. Introduction

Affordable housing continues to be a challenge in both developing and developed countries. Cement is the oldest and most reliable binding agent, since it can be used alone in any type of earth, achieving the desired properties [25]. Unfortunately, cement production (more so its precursor clinker) is responsible for significant global carbon dioxide emission and therefore, is not considered an environmentally sustainable product. Upgrading local materials presents an opportunity for delivery of affordable houses and reduction in the carbon dioxide emissions.

Over the last few decades, there has been an increasing trend of blending ordinary cement and lime with locally sourced raw materials that possess pozzolanic properties for making concrete blocks and compressed earth blocks (CEBs) [20]. Nagaraj et al. [22], who investigated the combination of cement with lime in the construction of CEBs, found out that addition of optimum quantity of lime

* Corresponding author at: Maseno University, P.O. Box Private Bag, Maseno, 40137, Kenya.
E-mail addresses: info@maseno.ac.ke (J. Ouma), principal@tmuc.ac.ke (N. Ongwen), ogam@lma.cnrs-mrs.fr (E. Ogam), fellah@lma.cnrs-mrs.fr (Z.E.A. Fellah), info@mmust.ac.ke (M. Mageto).

https://doi.org/10.1016/j.cscm.2023.e01828
Received 25 July 2022; Received in revised form 14 November 2022; Accepted 3 January 2023
Available online 4 January 2023

to cement produces CEBs that are mechanically stronger than those prepared using cement alone. Making of CEBs requires earth and a binder, although some studies, including that by Nagaraj et al. [21], have suggested the use of earth without physical modification or increasing the stabilizer content. However, binders improve the earth's geotechnical properties such as compressibility, strength, permeability, and durability [28]. Hydrated lime, while emitting carbon dioxide during the burning phase, reabsorbs equivalent amounts of carbon dioxide from the atmosphere, resulting in carbon neutral life cycle [1]. Therefore, replacing cement in the fabrication of CEBs with lime and locally sourced materials such as water hyacinth ash (WHA) would lead to reduced cost of construction, reduced greenhouse gas emission, reduced energy input, as well as solving the housing crisis.

CEBs are good sound absorbers, resistant to fire and insect damage, and durable if properly protected [2]. Therefore, it can be concluded that these blocks are energy-efficient and environmentally friendly. However, if the mixture of the ingredients for the manufacturing of these CEBs are not properly optimized and designed, it may lead to poor response when subjected to intense loading during seismic events, and may reach unacceptable performance levels, leading to structural collapse [23].

In this study, we investigated the effect of compaction pressure, WHA, and lime content on the macroscopic non-acoustical properties influenced by the porous skeleton microstructure (porosity, tortuosity, thermal characteristic length, and viscous characteristic length) and transport acoustical properties such as permeability (related to airflow resistivity) of CEBs. The objectives of the study were (i) to find out the effect of amount of WHA and lime on the acoustical properties of CEBs, and (ii) to find out the effect of compaction pressure on the acoustical (transmission coefficient) and non-acoustical macrostructural properties of CEBs.

2. Materials and methods

2.1. Sample preparation

This study was conducted systematically through a series of experiments as shown in Fig. 1. We used the following raw materials: natural site earth, lime, WHA, and water. The earth was obtained from Mayenje Ward, Matayos Sub-county in Busia county (Kenya) and then air-dried. A sieve test [5] was performed on the earth sample in order to determine its grain size distribution. Using the information obtained from the sieve test, the earth was classified using the process provided by Unified Soil Classification System-USCS (ASTM D2487, 2000). A typical commercial class A lime that complies with the requirements of specification [3] was used as testing lime.

The water hyacinth was collected from Dunga Beach in Kisumu County, Kenya. Fresh water hyacinth stems were obtained and then thoroughly washed with clean water in order to get rid of debris and other impurities. The clean water hyacinth stems were then cut into 2-inch pieces using a sharp table knife before being sundried for two weeks. The dried stems were thereafter incinerated in an oven at 800 °C for six hours in order to convert the organic matter into inorganic substance, and then ground using a laboratory scale ball mill for 30 min in order to form the WHA [10]. The ground WHA was finally passed through a 150-micrometer sieve as per IS: 1727–1967 in order to obtain the final WHA with fineness similar to that of Ordinary Portland Cement [20] (Fig. 2a).

The earth was sieved through an 8 mm aperture size sieve prior to the manufacture of the CEBs so as to retain particles whose sizes were less than 8 mm. The sieved earth was then oven-heated at 105 °C for 24 h in order to convert the organic matter into inorganic substance (Fig. 2b). The dried earth was then mechanically mixed with lime (Fig. 2c) and WHA, after which water was added and the mixing continued until the mixture became homogeneous (Mansour et. al., 2016). The volume of water added was determined using the drop test [12].

The mixture was then compacted in a cylindrical mold (the CEBs) of internal diameter 76 mm, which is equal to the internal diameter of the wave guide that was used for the acoustical characterization; and a height of 20 mm for them to be easily characterized in low frequency regime. The pressing was done using a hydraulic press (Hydraform, model number M7TWIND, South Africa). Four

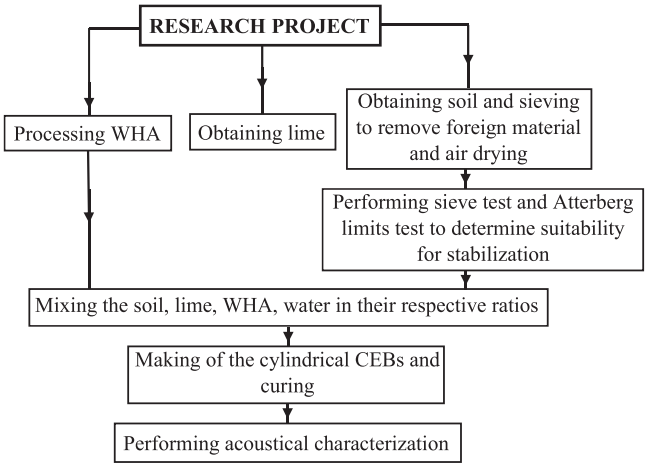

Fig. 1. Research framework for fabrication and acoustic characterization of CEBs.

Fig. 2. (a) The final WHA, ready for use; (b) The final sieved soil, ready for use; (c) The prepared lime; and (d) The prepared CEB samples.

replicates for each mix proportion (designated M-1 to M-4) were made (Table 1), all at a compaction pressure of 25 bars. The compaction pressure was then increased to 50, 75 and then 100 bars for the other samples. After compaction, the blocks were cured for 21 days under plastic sheeting for them to gain adequate mechanical strength for use in acoustical characterization. Fig. 2d shows the prepared CEB samples.

2.2. Acoustical characterization

After the CEBs had been dried, they were taken for the measurement of acoustic transmission coefficient, which was performed using a wave guide of length 17 m and an internal diameter 0.076 m. The cylindrical CEB samples made to fit exactly into the cross-

Table 1
Mix-proportions for earth, lime, WHA and water at a pressure of 25 bars. Other samples at 50 bars, 75 bars and 100 bars were also prepared.

Mix-designation	Pressure (bar)	Constituent material (% by mass)			Water (% mass of constituent material)	Replicates
		Soil	Lime	WHA		
M-1	25	90	10	0	30	4
M-2	25	90	7	3	25	4
M-3	25	90	5	5	40	4
M-4	25	90	3	7	30	4
M-5	50	90	10	0	30	4
M-6	50	90	7	3	25	4
M-7	50	90	5	5	40	4
M-8	50	90	3	7	30	4
M-9	75	90	10	0	30	4
M-10	75	90	7	3	25	4
M-11	75	90	5	5	30	4
M-12	75	90	3	7	30	4
M-13	100	90	10	0	25	4
M-14	100	90	7	3	40	4
M-15	100	90	5	5	30	4

section of the wave guide were inserted 3 m downstream of the acoustic source, one at a time. The edges of the samples were sealed using black tape. An omnidirectional microphone with integrated preamplifier was placed 12 m downstream of the pipe from the acoustic source (9 m from the CEBs sample) in order to capture both the incident and the transmitted signals. The useful frequency range of the waveguide was 18.8–2467.4 Hz, which was calculated according to the formula [24]:

$$f_L = \frac{v}{l + 1.6r}; f_H = \frac{1.8412v}{2\pi r}, \tag{1}$$

where v is the speed of sound in the fluid (air in this case, which was taken as 340 m/s), l is the length of the pipe (waveguide), r is the radius of the pipe, f_L is the low cut-off frequency of the waveguide, and f_H is the high cut-off frequency of the waveguide. The lower frequency limit could have been lowered further by lengthening the pipe. However, this is subject to the available free space in the experimental area. A transient sound wave was then generated in the waveguide by a ribbon loud speaker (VIAWAVE SRT-7, SN 32237, Petrozavodsk, Russia), which was in turn connected to a signal generator (Thurlby Thandar TG 210 function generator, Huntingdon. Cambs UK). The generator was programmed to produce a Heaviside signal (step function). The acoustic leakage between the edges of the samples and the pipe walls due to the sample not being perfectly circular was prevented using putty (brand and address). The incident signal was captured before inserting the specimen (sample CEBs), while the transmitted signal was captured with the specimen fitted into the waveguide. The response signals obtained was then digitized using a digital storage oscilloscope from pico technology (picoscope 4262, United Kingdom), with a maximum frequency of 5 MHz and a bit rate of 16 bits, connected to the microphone (Fig. 3).

Exploitation of the data and simulation of the model was realized using Julia programming language [7]. The transmission coefficient was obtained through the computation of the transfer function between the incident and transmitted acoustic signals. The transfer function $T_{IT}(f)$ is computed from the quotient of cross power spectral density S_{IT} of the incident $(P_I(t))$ and transmitted $(P_T(t))$ acoustic pressure and the power spectral density ($S_{II}$of $P_I(t)$) [24]:

$$T_{IT}(f) = \frac{S_{IT}(f)}{S_{II}(f)} \tag{2}$$

2.3. Solution of the inverse problem for determination of acoustical parameters

The analytical expression of the transmission coefficient for a porous rigid frame plate of infinite dimensions in the frequency domain considered in this work was derived from an earlier study by Mansour et al. [18] from the wave propagation equation. The equation is given by:

$$T^{EFM}(\omega) = \frac{2\phi x_r e^{iK_f d}}{i\left(x_r^2 + \phi^2\right)\sin(k_1 d) + 2x_r\phi\cos(k_1 d)}, \tag{3}$$

where T^{EFM} is the equivalent fluid model (EFM) transmission coefficient, $K_f = \omega/c_f$ is the wavenumber and c_f is the wave velocity in the fluid, k_1 is the wave number in the porous layer $\left(k_1(\omega) = \omega\sqrt{\frac{\rho_f \alpha(\omega)\gamma(\omega)}{K_f}}\right)$, $x_c = \rho_1 c_1$ is the characteristic specific acoustic impedance of the porous medium (c_1 is the wave velocity), $x_f = \rho_f c_f$ is that of free air, $x_r = x_c/x_f$ is their ratio, and $d = \triangle L$ is the thickness. The coefficient $\alpha(\omega)\gamma(\omega)$ is the refractive index of the medium that changes the wave velocity from $c_f = \left(\frac{\rho_f}{K_f}\right)^{-\frac{1}{2}}$ in free space to $c_1(\omega) = \frac{c_f}{\sqrt{\alpha(\omega)\gamma(\omega)}}$ in the porous medium.

The frame models of the dynamic tortuosity by Johnson et al. [14], and the dynamic compressibility modeled by Champoux and Allard [9], and later improved by Lafarge [15] (also known as JCAL) were chosen because they provide a complete description of the inertial, viscous, and thermal interactions in the porous earth blocks. They are the dynamic tortuosity ($\alpha(\omega)$) and the dynamic compressibility, modify respectively, the fluid density (ρ_f) and the fluid compressibility (K_f) through the multiplier process to obtain the modified parameters of the porous medium in the frequency domain ($\rho_1 = \rho_f\alpha(\omega)$ and $K_1 = K_f\gamma(\omega)^{-1}$).

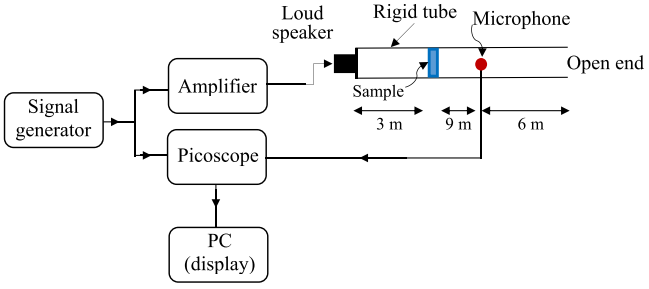

Fig. 3. The experimental set up for the acoustic measurement of transmission coefficient of the samples.

$$\alpha(\omega) = \alpha_\infty \left(1 + \frac{\lambda\phi}{i\omega\alpha_\infty \rho_f k_0} \sqrt{1 + i\frac{4\alpha_\infty^2 k_0^2 \rho_f \omega}{\lambda\Lambda^2\phi^2}}\right) \tag{4}$$

$$\gamma(\omega) = \vartheta - (1-\vartheta)x\left(1 + \frac{\lambda\phi}{i\omega\rho_f k_0' P_r} \sqrt{1 + i\frac{4k_0'^2 \rho_f \omega P_r}{\lambda\Lambda' 2\phi^2}}\right), \tag{5}$$

with $i = \sqrt{-1}$, λ is the viscosity, ϕ and α_∞ are respectively, the porosity and tortuosity of the porous medium, Λ and Λ' are the viscous and thermal characteristic lengths, ρ_f is the density of the fluid, P_r is the Prandtl number. The static viscous permeability ($k_0 = \lambda/\sigma$) is an intrinsic parameter that depends only on the geometry of the pores (σ is the airflow resistivity). k_0' is the static thermal permeability [16], which partly characterizes the thermal effects at low frequencies.

The inverse problem (IP) of an acoustic wave transmission by a porous material in this study involved the retrieval of the six acoustic wave parameters (ϕ, σ, Λ, α_∞, Λ'/Λ and k_0') from the measured transmission coefficient of a porous slab in a long pipe and an acoustic/CEB interaction model of wave transmission using an EFM. An error functional that expresses the distance between the transmission coefficient data and the interaction model, and from the experiment was computed for each set of trial values of the six microgeometry and transport acoustical parameters. Choosing the functional F that expresses this discrepancy was:

$$F(\omega, \phi, \sigma, \Lambda, \alpha_\infty, \Lambda' \Big/ \Lambda, k_0') = \sum_{n=1}^{N} \left(\left|T^{EFM}(\omega, \phi, \sigma, \Lambda, \alpha_\infty, \Lambda'/\Lambda, k_0')\right| - \left|T_{IT}^{exp}(\omega)\right|\right)^2 \tag{6}$$

Here, T_{IT}^{exp} denotes the transmission coefficient obtained from the experimental data. Through minimization of the objective functional F, the six acoustical parameters were retrieved. The minima were found through varying the acoustical model parameters at small intervals [29]: ϕ was varied at interval of 0.01, σ at 200, Λ at 2.0×10^{-6}, α_∞ at 0.01, Λ'/Λ at 0.01, and k_0' at 1.0×10^{-10}. The solutions of the acoustical parameters were obtained at the global minima of the cost functions against the respective acoustical parameters [17]. The process was done for each parameter at a time (since it is manual), while keeping the others fixed [18].

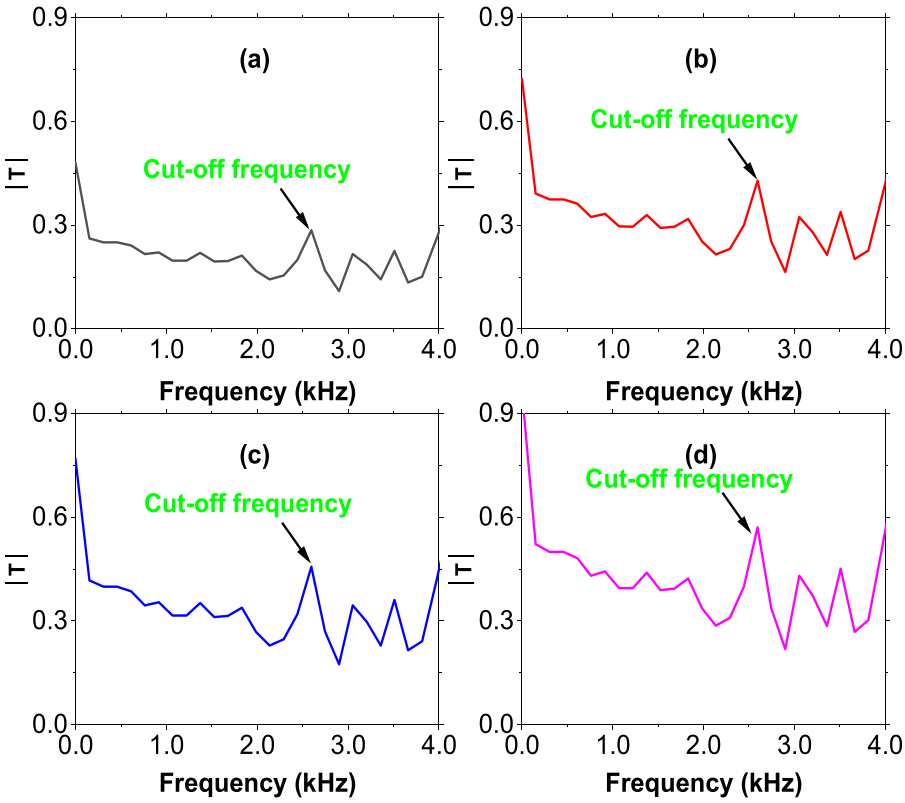

Fig. 4. Transmission coefficient of the CEBs samples at a pressure of 25 bars, with the soil at 90 %. (a) 10 % lime and 0 % WHA; (b) 7 % lime and 3 % WHA; (c) 5 % lime and 5 % WHA; and (d) 3 % lime and 7 % WHA.

3. Results and discussion

3.1. Effect of WHA and lime concentrations on the acoustic transmission coefficient

The change in the transmission coefficients of the CEBs (samples M-1 to M-4) with the variation in WHA and lime are shown in Fig. 4, all prepared at a compaction pressure of 25 bars. As the figure depicts, an increase in the WHA content leads to a consistent corresponding increase in the transmission coefficient in all the four samples. This implies that WHA has the effect of increasing the porosity of the CEBs. When lime is added to soil, the soil properties change. There is a consistent increase in the transmission coefficient with reduction in the lime content. According to Bell [6], when the calcium ion in the lime reacts with soil, metallic ion and cation exchange between them takes place. Thus, the soil particles are surrounded by a diffuse hydrous double layer. This causes an alteration in the electrical charge density around the soil particles that make the particles closer and form flocks in a process known as flocculation. Flocculation results to a decrease in the transmission coefficient.

The curves are relatively linear up to the cut-off frequency, after which oscillations start to occur. A peak is observed near a frequency of 2500 Hz for all the graphs, which is close to the theoretical upper cut-off frequency of the waveguide (2467.4 Hz). Beyond 2500 Hz, the waves are no longer plane waves. Therefore, the useful bandwidth is from 18.8 to 2500 Hz. Fig. 4 also shows that as the frequency approaches 0 Hz, the transmission coefficient approaches 1.

3.2. Effect of compaction pressure on the transmission coefficient

Fig. 5 shows the variation of the transmission coefficient of samples M-2, M-6, M-10 and M-14 with frequency (chosen as an example). It is observed that as the compaction pressure applied increased, the transmission coefficient decreased. This is because as the compaction pressure increases, the granular packaging of the blocks and the fluid phases re-arrange themselves. This leads to a decrease in the number of macroscopic pores. This modification results into a decrease in the magnitude of the transmission coefficient. The same reduction in the transmission coefficient with increase in the compaction pressure has been reported (Mansour et. al, 2016).

3.3. Effect of non-acoustical parameters on the concentration of WHA and lime

The plots of the cost functions against the sought-for acoustical parameters (porosity, airflow resistivity, tortuosity, viscous characteristic length, thermal characteristic length, the ratio between viscous and thermal characteristic lengths, and thermal permeability) for sample M-4 (chosen as an example) is shown in Fig. 6. The values of the sought-for parameters were obtained from the minima of the curves. As can be observed, unique minima around the intervals of the solutions were obtained for all the six sought-for parameters.

From the minima of the cost function curves, Fig. 7 was obtained through plotting of the retrieved values of the macroscopic parameters describing the microstructure i.e., the non-acoustical parameters of the blocks compacted at a pressure of 25 bars for samples M-1 to M-4 (0–10 % WHA). There is a linear increase in the porosity with increase in the WHA content from 0.52 to 0.88 (Fig. 7a), but airflow resistivity decreased from 89,400 Pa.s.m^2 to 17,600 Pa.s.m^2 (Fig. 7b). The decrease in the airflow resistivity with increase in the composition of WHA can be attributed to the increase in the porosity (as observed in Fig. 7a), which leads to increase in the sizes of the voids.

The variation of tortuosity with the concentration of WHA is shown in Fig. 7c, which shows an increase from 1.68 to 4.00 with increase in WHA. The tortuosity of granular materials range between 1 and 1.5. For other construction materials such as concrete, the value goes up to 3.5, which is due to the shape of the particles as well as the orientation facing the airflow, making a tortious path. An increase in the WHA content leads to a corresponding increase in the viscous characteristic length of the samples, as shown in Fig. 7d. This is quite in agreement with the results of the porosity (Fig. 7a), since a higher value of the viscous characteristic length leads to an increase in the size of the voids, thus increasing the porosity. Fig. 7e shows the static thermal permeability, which is equal to the inverse trapping constant of the solid frame. This parameter describes the thermal exchanges between the frame and saturating fluid [18]. As can be observed, the thermal permeability increases with increase in the concentration of WHA. Fig. 8f shows that the static

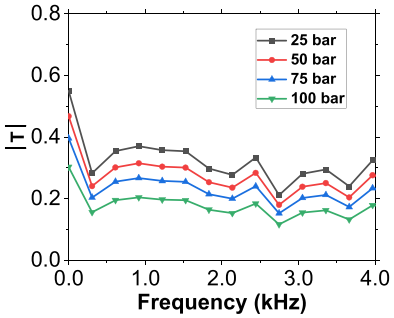

Fig. 5. Effect of compaction pressure on the acoustic transmission coefficient of the CEBs (samples M-2, M-6, M-10 and M-14).

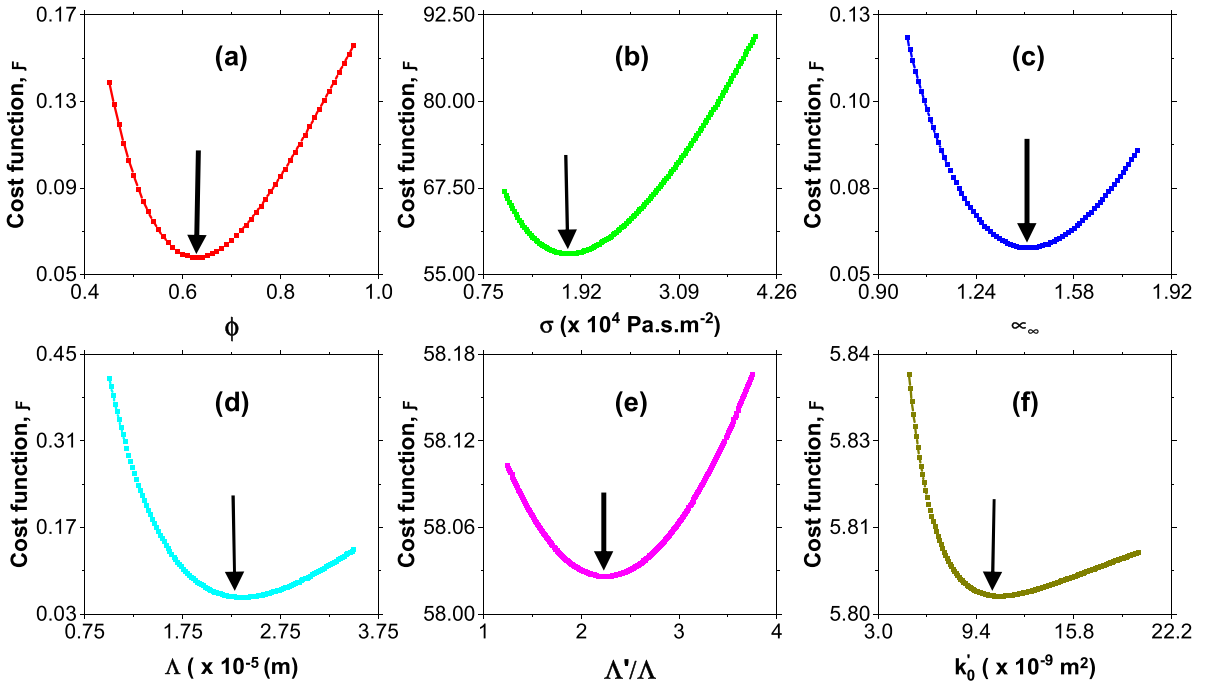

Fig. 6. Plots of cost functional Ƒ against the sought-for acoustical parameters for sample M-4: (a) Porosity (ϕ), (b) Airflow resistivity (σ), (c) Tortuosity ($\propto_\infty$), (d) Viscous characteristic length (Λ), (e) ratio (Λ'/Λ), and (f) thermal permeability (k_0'). The arrows indicate the minimum that gives the parameter values.

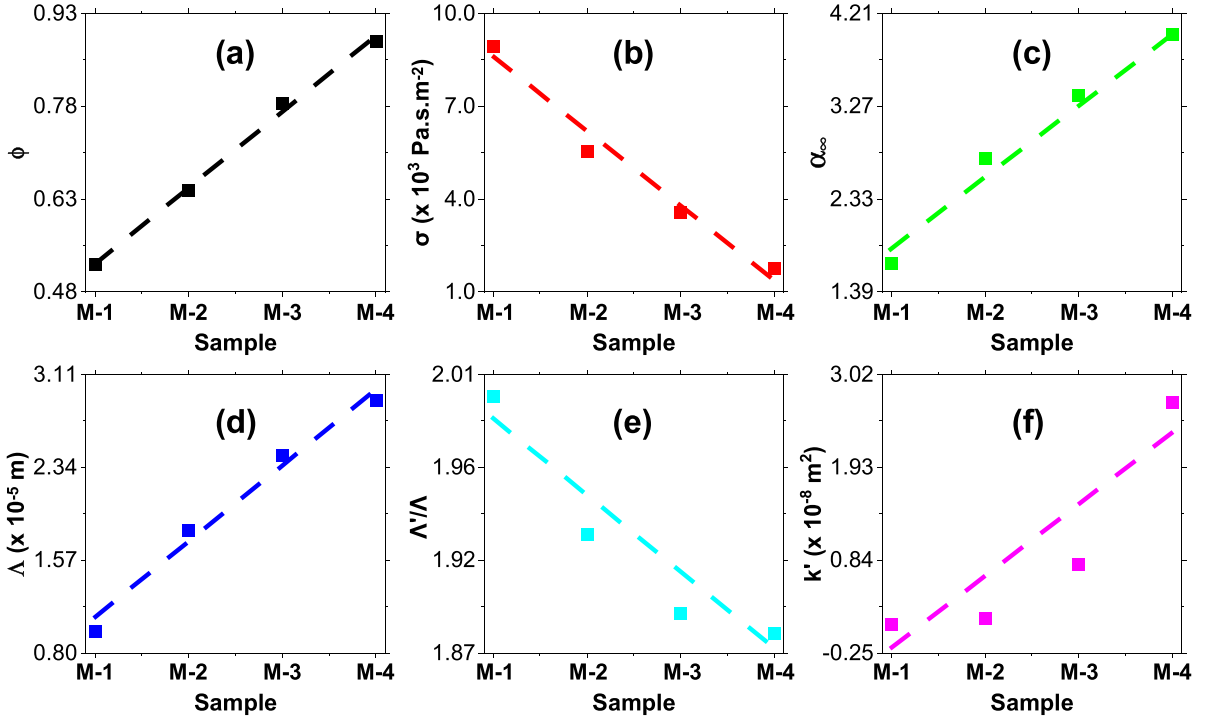

Fig. 7. Plots of the non-acoustical parameters: (a) porosity, ϕ; (b) airflow resistivity σ; (c) tortuosity α_∞; (d) viscous characteristic length (e) the ratio between thermal characteristic length Λ' and viscous characteristic length Λ; (f) thermal permeability (k_0') against the sample number (from M-1 to M-4), all at a compaction pressure of 25 bars.

viscous permeability increases with increase in WHA, which is expected, since it is inversely proportional to the airflow resistivity.

Fig. 8 shows the variation of the microstructural non-acoustical parameters of the blocks as a function of the compression pressure and concentration of WHA. While the porosity increased with increase in the concentration of WHA, it decreased with increase in the compaction pressure (Fig. 8a). This can be attributed to the decrease in the volume of the voids with increase in the compaction pressure. Venkatarama [28] also reported the decrease in the porosity of CEBs with increase in the compaction pressure. The airflow resistivity increased with increase in the compaction pressure (Fig. 8b). This increase in air resistivity can be explained by the decrease in the porosity and decrease in the pore size as compaction pressure increases.

The high frequency parameters (tortuosity, viscous characteristic lengths and thermal permeability) could not be obtained with enough precision for compaction pressures higher than 25 bars, because the data involved was not sensitive enough to reflect their variation in order to recover them correctly. The viscous characteristic length of the CEBs decreases with increase in compaction pressure. This is due to the fact that increasing the compaction pressure reduces the volume of voids, increases the contact surface between the grains and subsequently leads to a reduction in pore size thereby decreasing the Λ. This results in a poor signal to noise ratio for these high frequency parameters. They also require more data points.

4. Conclusion

A simple acoustic test-rig using water pipes to form a long waveguide was built to characterize the acoustical parameters of CEB samples with varying percentages of lime and WHA. The study found out that the two binders did not behave in the same manner. Adding WHA to the CEBs was found to increase the transmission coefficient, porosity, tortuosity, viscous characteristic length, and static thermal permeability, but reduced the airflow resistivity. A linear increase in porosity was observed with increase in the WHA content. On the other hand, addition of lime to the CEBs reduced the transmission coefficient, porosity, tortuosity, viscous characteristic length, and static thermal permeability, but increased the airflow resistivity. Increase in the compaction pressure decreased the transmission coefficient and porosity, but increased the airflow resistivity. Thus, both the acoustical and non-acoustical properties of the CEBs can be tailored at low values of the compaction pressure. However, at high pressures, the model does not give a clear trend in the properties of the blocks because of the poor signal-to-noise ratio.

Funding

This research received funding from the Direction Europe de la recherche et coopération internationale (DERCI) AMOI-CNRS, in the framework of the Programme “Dispositif de Soutien aux Collaborations avec l’Afrique sub-saharienne, 2022–2024″.

CRediT authorship contribution statement

Justus Ouma: gathered the raw materials, carried out the experiment. Nicholas Ongwen: conceptualized the paper, carried out the experiment, analyzed the results and wrote the paper. Erick Ogam: conceptualized the paper, supervised the experiment, wrote the Julia script, analyzed the results. Z. E. A Fellah: analyzed the results and proofread the paper. Maxwell Mageto: conceptualized and proofread the paper. Mohamed Benmansour: conceptualized and proofread the paper, Andrew Oduor: proofread the paper. Mercy Auma: labelled the samples and collected the data.

Declaration of Competing Interest

The authors declare that they have no known competing financial interests or personal relationships that could have appeared to influence the work reported in this paper.

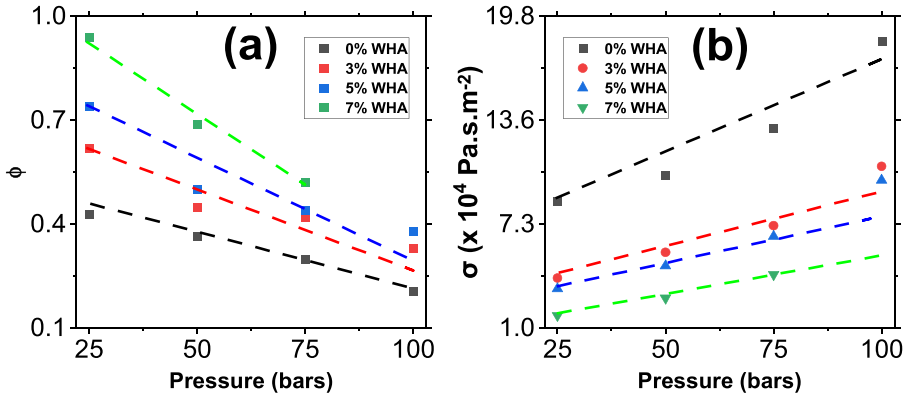

Fig. 8. Plots of the non-acoustical parameters: (a) porosity ϕ, and (b) airflow resistivity σ against compaction pressure.

Data Availability

Data will be made available on request.

Acknowledgement

The authors would like to acknowledge the Department of Housing, Ministry of Lands, Busia County (Kenya) for providing the hydraulic compressing machine that was used in preparing the samples. Special thanks also go to Gwendoline Ogam (architect) for the fruitful discussion on the binders.

References

[1] R. Alavez-Ramirez, P. Montes-Garcia, J. Martínez-Reyes, D.C. Altamirano-Juárez, Y. Gochi-Ponce, The use of sugarcane bagasse ash and lime to improve the durability and mechanical properties of compacted soil blocks, Constr. Build. Mater. 34 (2012) 296–305, https://doi.org/10.1016/j.conbuildmat.2012.02.072.
[2] Arumala, J. & Gondal, T. (2007). Compressed earth building blocks for affordable housing. The construction and building research conference of the Royal Institution of Chartered Surveyors, London, 6–7 September 2007. RICS.
[3] ASTM C110-20, Standard Test Methods for Physical Testing of Quicklime, Hydrated Lime, and Limestone, American Society for Testing and Materials, 2020.
[5] ASTM D422-63, Standard Test Methods for Particle-size Analysis of Soils, American Society for Testing and Materials, 2007.
[6] F.G. Bell, Lime stabilization of clay minerals and soils, Eng. Geol. 42 (4) (1996) 223–237.
[7] J. Bezanson, S. Karpinski, V.B. Shah, A. Edelman, Julia: A fast dynamic language for technical computing (2012), https://doi.org/10.48550/arXiv.1209.5145.
[9] Y. Champoux, J.-F. Allard, Dynamic tortuosity and bulk modulus in air-saturated porous media, J. Appl. Phys. 70 (1991) 1975–1979.
[10] N. Dash, S. Singh, Evaluation of water hyacinth stem ash as pozzolanic material for use in blended cement, J. Civ. Eng. Sci. Technol. 7 (1) (2016) 1–8.
[12] I.L. Ipinge, *Durability of compressed stabilized earth blocks*. (Master's thesis and dissertation), Johannesbg.: Univ. Witwatersrand (2012).
[14] D.L. Johnson, J. Koplik, R. Dashen, Theory of dynamic permeability and tortuosity in fluid-saturated porous media, J. Fluid Mech. 176 (1987) 379–402.
[15] D. Lafarge, Sound propagation in porous materials having a rigid frame saturated by gas. [Unpublished doctoral dissertation], Universit du Maine, Le Mans (1993).
[16] D. Lafarge, P. Lemarinier, J.-F. Allard, V. Tarnow, Dynamic compressibility of air in porous structures at audible frequencies, J. Acoust. Soc. Am. 102 (4) (1997) 1995–2006.
[17] G. Lefeuve-Mesgouez, A. Mesgouez, E. Ogam, T. Scotti, A. Wirgin, Retrieval of the physical properties of an anelastic solid half space from seismic data, J. Appl. Geophys. 88 (2013) 70–82.
[18] M.B. Mansour, E. Ogam, Z.E.,A. Fellah, S.C. Amel, J. Ahmed, S.B. Jabrallah, Characterization of compressed earth blocks using low frequency guided acoustic waves, J. Acoust. Soc. Am. 139 (5) (2016) 2551–2560, https://doi.org/10.1121/1.4948573.
[20] V. Murugesh, N. Balasundaram, Experimental investigation on water hyacinth ash as the partial replacement of cement in concrete, Int. J. Civ. Eng. Technol. (IJCIET) 8 (9) (2017) 1013–1018.
[21] H.B. Nagaraj, A. Rajesh, M.V. Sravan, Influence of soil gradation, proportion and combination of admixtures on the properties and durability of CSEBs, Constr. Build. Mater. 110 (2016) 135–144, https://doi.org/10.1016/j.conbuildmat.2016.02.023.
[22] H.B. Nagaraj, M.V. Sravan, T.G. Arun, K.S. Jagadish, Role of lime with cement in long-term strength of compressed stabilized earth blocks, Int. J. Sustain. Built Environ. 3 (1) (2014) 54–61, https://doi.org/10.1016/j.ijsbe.2014.03.001.
[23] L. Ocola, P. Huaco, Seismic response of adobe buildings in Peruvian territory;1974-2001 earthquakes, Proc. SismoAdobe2005 [CD-ROM], Lima (2005).
[24] E. Ogam, Z.E.A. Fellah, G. Ogam, N.O. Ongwen, A.O. Oduor, Investigation of long acoustic waveguides for the very low frequency characterization of monolayer and stratified air-saturated poroelastic materials, Appl. Acoust. 182 (108200) (2021) 1–13.
[25] P. Sherwood. Soil Stabilization with Cement and Lime: State of the Art Review, Transport Research Laboratory, HMSO, London, 1993.
[28] R.B.V. Venkatarama, Stabilised Soil Blocks for Structural Masonry in Earth Construction, Sawston: Wood Head Publishing Limited., 2012.
[29] A. Wirgin, Retrieval of the equivalent acoustic constitutive parameters of an inhomogeneous fluid-like object by nonlinear full waveform inversion, Ultrasonics 65 (2016) 353–369, https://doi.org/10.1016/j.ultras.2015.09.005.